ELSEVIER

Journal of Nuclear Materials 307–311 (2002) 1021–1025

journal of nuclear materials

www.elsevier.com/locate/jnucmat

Towards a micro-mechanical description of the fracture behaviour for RAFM steels in the ductile-to-brittle transition regime

Heinz Riesch-Oppermann *, Eberhard Diegele

Forschungszentrum Karlsruhe, Institut für Materialforschung II, P.O. Box 3640, D-76021 Karlsruhe, Germany

Abstract

A combined experimental and continuum mechanics approach is used to interpret cleavage fracture results of the F82Hmod reduced activation steel. Cleavage fracture parameters are obtained by numerical evaluation of tensile tests using axisymmetrically notched and pre-cracked specimens and subsequent statistical analysis. Prediction of fracture origin distribution was performed using the cleavage fracture results and fractographic examinations were used to compare prediction and experimental results. The local risk of rupture is defined and utilized as quantity for transferability assessment between different specimen geometries. The role of large strains preceding cleavage fracture is addressed. While results are very satisfactory for small fracture strains, the presence of large strains and transferability to pre-cracked specimens poses some difficulties. A possible explanation for this is given.

1. Introduction

New 7–10% Cr-WVTa ferritic-martensitic steels with reduced generation of long-lived radionuclides following neutron irradiation (RAFM steels) have been developed during the last years as candidate structural material for components in nuclear fusion reactors. In particular, behaviour in the ductile-to-brittle transition regime is of concern because of the expected shift of the ductile-to-brittle transition temperature following neutron irradiation under in-service conditions.

Within the framework of the European Fusion Programme a comprehensive experimental and numerical programme has been established aimed at a micro-mechanics description of the ductile-to-brittle transition behaviour in the unirradiated condition. Future irradiated material behaviour description shall be based on these results. As a final goal, fracture mechanics guidelines shall be obtained as part of a design code.

The paper addresses transferability of test results using an integrated (i.e., combined experimental and continuum mechanics) approach which is based on the 'local approach' to fracture [1].

Tensile test results on notched and pre-cracked specimens together with fractographic examinations are used for the characterization of fracture behaviour [2]. Cleavage fracture parameters are obtained by finite element evaluation of the stress field at fracture and subsequent statistical inference of the test sample results [3]. For transferability assessment between different specimen geometries and test temperatures, the local risk of rupture is presented and used in the paper. Fractographic examinations are used to verify the predictions. Results are presented for the Japanese F82Hmod reduced activation steel.

2. Material

The composition of the material is given in Table 1. The material is available in a reference heat treatment condition of 1040 °C/38 min+750 °C/60 min with a DBTT observed in Charpy V impact tests of about −70

* Corresponding author. Tel.: +49-7247 82 4155; fax: +49-7247 82 2347.

E-mail address: riesch-oppermann@imf.fzk.de (H. Riesch-Oppermann).

0022-3115/02/$ - see front matter
PII: S0022-3115(02)01257-6

Table 1
Composition (wt%) of F82Hmod, data are from heat no. 9741

C	0.09
Si	0.11
Mn	0.16
P	0.002
S	0.002
Cu	0.01
Ni	0.02
Cr	7.66
Mo	0.01
V	0.16
Nb	0.01
B	0.0002
T.N	0.005
Sol. Al	0.001
Co	0.01
Ti	0.001
Ta	0.02
W	2.00

to −50 °C [4]. The microstructure is fully martensitic with a grain size of about 70 μm and no significant difference in LT, LS and TS orientation.

3. Experiments and numerical analyses

Following a numerical analysis of the stress/strain fields, axisymmetrical notched tensile specimens with various notch dimensions were fabricated and tested at −150, −75 °C, and ambient temperature. The tests were performed under displacement control with a crosshead speed of 0.5 mm/min and continuous optical recording of the minimum notch diameter, d. The measured diameter reductions at fracture, Δd, were used as loading parameter for the subsequent calculation of the Weibull stress at fracture, σ_W. σ_W is given as result of a numerical integration of the stress field at fracture according to

$$\sigma_W^m = \frac{1}{V_0}\int_{V_{pl}} \sigma_1^m \, dV, \tag{1}$$

where m is the so-called Weibull modulus, V_0 is a reference volume introduced for dimensional purposes only, and σ_1 is the first principal stress at fracture. The integral is evaluated over the plastic volume, V_{pl}, of the specimen [3]. The Weibull stress at fracture is a Weibull-distributed random variate, whose distribution parameters (m, σ_u) are obtained from a given sample by an iterative maximum likelihood procedure [5]. A Weibull stress analysis of 1 and 2 mm notched specimens tested at −150 °C was used for the subsequent analysis of the local risk of rupture predictions. In statistical terms, we obtain the local risk of rupture as conditional probability of having a micro-crack in some sub-volume, V_s, of the specimen under the condition that this micro-crack causes unstable fracture. If A denotes the event that a micro-crack is located within a certain sub-volume, V_s, and B denotes the event that a given micro-crack causes failure, the conditional probability $P(A|B)$, i.e. the probability that a certain micro-crack that causes fracture is located within sub-volume V_s, is obtained as [2]

$$P(A|B) = \frac{\int_{V_s} \sigma_1^m \, dV}{V_0 \sigma_W^m}. \tag{2}$$

Eq. (2) shows that $P(A|B)$ depends only on the scatter of the Weibull stress σ_W, which is characterized by the Weibull modulus, m, but not on its characteristic value, σ_u. For $V_s \to 0$, we obtain a conditional probability density $\pi_i(\vec{x}|\sigma_W)$ which characterizes the local risk of rupture at load level i with a Weibull stress of $\sigma_W(i)$:

$$\pi_i(\vec{x}|\sigma_W) = \frac{\sigma_1^m(\vec{x}, i)}{V_0 \sigma_W^m(i)}. \tag{3}$$

For comparison with experimental findings, Eq. (3) has to be integrated over the whole Weibull stress range. The obtained integrated local risk of rupture $\pi(\vec{x})$ at location $\vec{x}$ corresponds to the fracture origin location distribution and is given as a convolution integral according to the following formula [2]:

$$\pi(\vec{x}) = \int_0^\infty \pi_i(\vec{x}|\sigma_W) f_{\sigma_W}(\sigma_W) \, d\sigma_W. \tag{4}$$

Eq. (4) contains the probability density $\pi_i(\cdot)$ of the fracture locus at load level i which is obtained by finite element analyses [2]. The probability density $f_{\sigma_W}(\cdot)$ of the Weibull stress at fracture is the Weibull distribution with parameters (m, σ_u). Eq. (4) is solved by numerical integration. Appropriate choice of the upper bound of the integration domain can be confirmed by checking the normalization condition

$$\int_V \pi(\vec{x}) \, dV = 1 \tag{5}$$

which has to be satisfied due to the fact the integrated local risk of rupture $\pi(\cdot)$ constitutes a probability density over V, namely the probability density of the fracture origin distribution within the specimen. Values of $\pi(\cdot)$ are available at each integration point of the finite element model. Graphical visualization of the results (see below) was obtained by generating a neutral output file for the FEMGV FE-post-processor program.

4. Results

Table 2 shows results of the Weibull stress parameters obtained for various geometries and temperatures. Two groups of results can be identified. The first group, associated with small fracture strains, exhibits moderate

Table 2
Results for σ_W distribution parameters (m, σ_u) and respective maximum likelihood confidence intervals

T (°C)	r (mm)	m	90% ML-CI	σ_u (MPa)	90% ML-CI
−150	1	11.6	[8.2, 16.6]	1943	[1867, 2022]
	2	10.7	[7.5, 15.3]	2106	[2019, 2200]
	5	78.9	[50.8, 124.5]	1913	[1900, 1927]
−75	1	107.5	[69.2, 169.5]	1941	[1928, 1955]
	2	78.8	[50.8, 124.3]	1765	[1752, 1777]
	5	–	–	–	–

values of m, whereas for the second group, associated with large fracture strains, m attains values of about 80–100. Complementary fractographic investigations on flat notched tensile specimens at ambient temperature revealed that, with increasing plastic deformation, martensite laths tend to orient themselves in loading direction [2]. For large strains, plastic deformation leads to pronounced formation of micro-cracks along the carbide-decorated martensite laths and former austenite grain boundaries (axial cracking) that is clearly visible on fracture surfaces. Obviously this behaviour is not restricted to ambient temperature, (see Fig. 1 for a view on the fracture surface of a 5 mm notched specimen tested at −150 °C) but is a consequence of large fracture strains. Axial cracking coincides with unusually large values of the Weibull modulus, m, as given in Table 2 and is thus characteristic for shallowly notched specimen geometries and/or higher temperatures, where large fracture strains are present. The extraordinary high values of the Weibull modulus, m, indicate a localized fracture event which is not characterized by weakest link failure but rather by a strain localization mechanism with subsequent trans/intergranular cleavage fracture.

Presence of different fracture mechanisms certainly poses severe difficulties in transferability of results between different geometries. For cases where weakest link failure takes place transferability of results between different geometries should be possible. For the comparison between the numerical approach and the experimentally observed fracture behaviour, the fracture origin location distribution is used which is available from fractographic investigations. Prediction of the fracture origin location distribution is possible according to Eq. (4) using the Weibull stress results of a reference data set as given by Eq. (1). For the calculation, Weibull parameters of the specimens tested at −150 °C are used as reference values. Results of the prediction for the 1 and 2 mm notched specimens, respectively, are given in Fig. 2(a) and (b). The predictions correspond well with results from quantitative fractography which are shown in Fig. 3(a) and (b), indicating that the numerical approach is appropriate.

A series of additional tensile tests on flat notched specimens was conducted at room temperature in order to identify the fracture process on a microscopic scale. These tests showed that, with increasing plastic deformation, martensite laths tend to orient themselves in loading direction. This can be observed from Fig. 4, where two regions are shown, the first one (Fig. 4(a)) located at some distance from the notch, where plastic

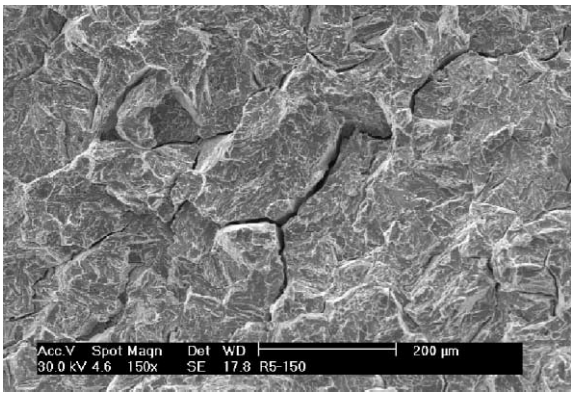

Fig. 1. Fracture of 5 mm notched specimen tested at −150 °C.

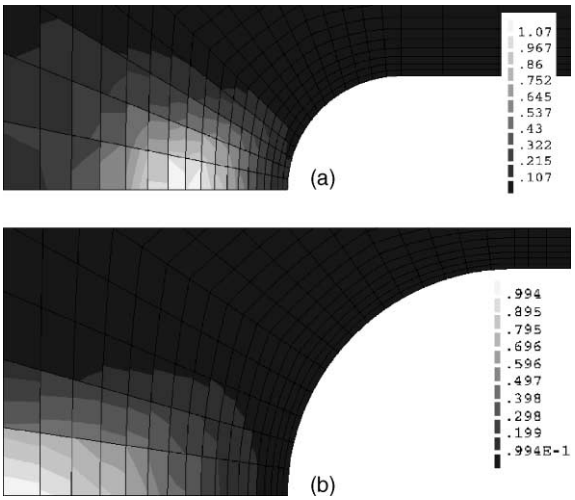

Fig. 2. Local risk of rupture at −150 °C; (a) $r = 1$ mm notched specimens, (b) $r = 2$ mm notched specimens.

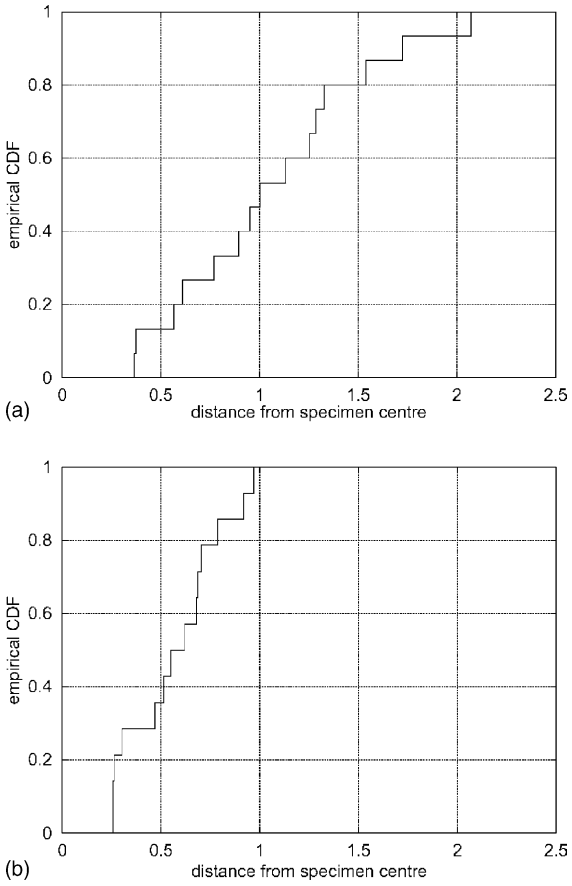

Fig. 3. Fracture origin distributions from fractographic examinations of specimens tested at −150 °C; (a) $r = 1$ mm notched specimens, (b) $r = 2$ mm notched specimens.

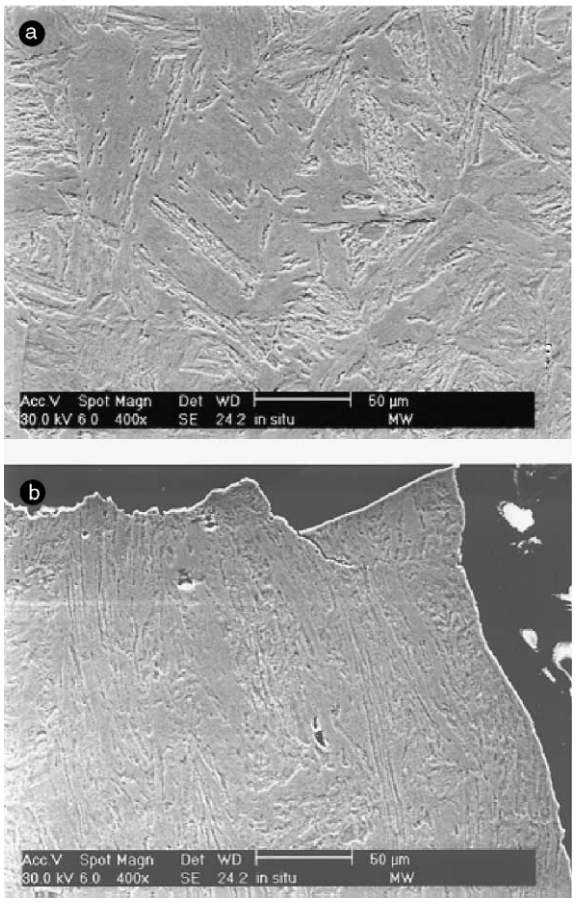

Fig. 4. Orientation of martensite laths in (a) undeformed and (b) deformed part of the specimen.

deformation is negligible, the second one (Fig. 4(b)) located in the vicinity of the notch. The different orientation of the carbide decorations indicating the martensite laths is clearly visible. Change in orientation is connected with shear stresses acting on carbide decorated martensite laths so that finally cracks may become able to initiate. We attribute the origin of cracks as shown in Fig. 1 to the same kind of shear-controlled crack initiation mechanism which is not only present at ambient temperature but also is active at low temperature provided that sufficient plastic deformation is occurring.

For pre-cracked specimens at −150 °C, the predicted local risk of rupture density is confined to a small region of less than 50 μm ahead of the crack tip as shown in Fig. 5, whereas the observed fracture origin locations are located about 2–8 grain diameters (150–500 μm) from the crack tip. This discrepancy may be due to the pronounced stress gradients of the crack tip field, which where neglected in the fracture mechanics model leading to the Weibull stress of Eq. (1).

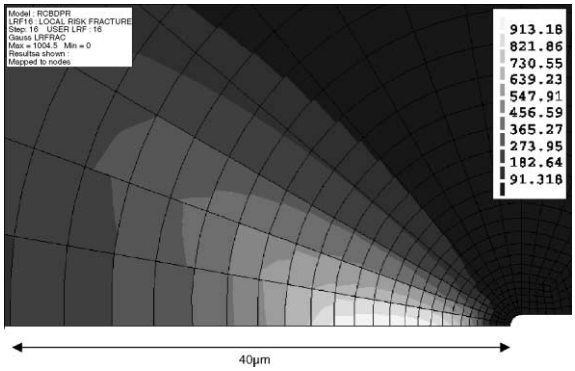

Fig. 5. Local risk of rupture density for pre-cracked specimen (material parameters correspond to −150 °C).

5. Conclusions

Cleavage fracture of F82Hmod RAFM steel was investigated using an integrated (combined experimental

and continuum mechanics) approach. Cleavage fracture parameters were identified by FE analysis of notched tensile specimens. For transferability analysis, a subsequent prediction of the fracture origin distribution for notched specimens was performed and results were compared with fractography of fractured specimens. Agreement was satisfactory in case of small fracture strains. For larger strains at fracture, the fracture mode changed to strain-induced axial cracking which poses some problems in transferability of results. For pre-cracked specimens, the predicted local risk of rupture was confined to a very small zone ahead of the crack tip which was not the case in the experiments and may explain why prediction of pre-cracked specimens from notched specimens is difficult.

Acknowledgements

Conduction of tensile tests and fractographic examinations by M. Walter (Forschungszentrum Karlsruhe) is gratefully acknowledged. The work performed by the Association Forschungszentrum Karlsruhe/EURATOM is supported by the European Community within the 5th Framework Fusion Technology Programme under task ID TTMS-005.

References

[1] F.M. Beremin, Metall. Trans. 14A (1983) 2277.
[2] H. Riesch-Oppermann, M. Walter, Status report on experiments and modelling of the cleavage fracture behaviour of F82Hmod using local fracture criteria, Forschungszentrum Karlsruhe, Report FZKA 6388, 2001 (available online under: http://bibliothek.fzk.de/zb/berichte/FZKA6388.pdf).
[3] H. Riesch-Oppermann, A. Brückner-Foit, WEISTRABA – A code for the numerical analysis of Weibull stress parameters from ABAQUS finite element stress analyses, Forschungszentrum Karlsruhe, Report FZKA 6155, 1998.
[4] M. Rieth, Forschungszentrum Karlsruhe, personal communication.
[5] F. Minami, A. Brückner-Foit, D. Munz, B. Trolldenier, Int. J. Fract. 54 (1992) 197.